Polymer Chemistry

ROYAL SOCIETY OF CHEMISTRY

PAPER

View Article Online
View Journal | View Issue

Cite this: *Polym. Chem.*, 2025, **16**, 3835

Expanding the chemical functionality of levoglucosenone-based monomers for degradable thiol–ene thermosets with high bio-derived content†

Mahesh Prasad Timilsina, [a] Melissa K. Stanfield, [a,b] Jason A. Smith [a] and Stuart C. Thickett *[a]

Levoglucosenol, the reduced form of levoglucosenone (LGO), was utilized in this work to synthesize seven novel monomers bearing both pendant alkene functional groups and the inherent internal double bond of the bicyclic LGO structure. Monomers possessing ester, carbonate and carbamate linkers were prepared with a specific focus on developing compounds with a high fraction of bio-derived carbon, which was achieved using fatty acids (oleic and linoleic acid) and plant-based acids (citronellic and 10-undecenoic acid). The monomers were cured *via* ultraviolet (UV)-initiated radical thiol–ene "click" chemistry with commercially available multifunctional thiols generating optically transparent cross-linked thermosets in typically less than 60 seconds, and which possessed tuneable thermal and mechanical properties. Thermogravimetric analysis revealed that most polymers were stable up to 300 °C, with glass transition temperatures ranging from 0.3 to 37.4 °C and tensile strength values varying from 0.5 to 54.0 MPa, depending on the nature of the structure of the LGO-based monomer. The hydrolytic degradation of these thermosets *via* ester hydrolysis was demonstrated in an alkaline medium, the rate of which could be controlled by the length of the monomer side chain and nature of the linker unit.

Received 4th April 2025,
Accepted 23rd July 2025

DOI: 10.1039/d5py00339c

rsc.li/polymers

Introduction

Society has benefited significantly from the creation of polymeric materials that have given comfort to human beings in various applications in everyday life, ranging from commodity plastics to high-performance materials. However, the polymer industry has relied heavily on fossil-fuel-based resources that are non-renewable and their isolation and extraction can lead to significant environmental consequences.[1–3] Furthermore, numerous classes of polymers persist in the natural environment for an extended period as their structure often prevents degradation.[4] To address the negative impact of these fossil-fuel-based products, there has been a significant effort to move towards designing polymers from renewable sources of monomer feedstocks, such as biomass, to create eco-friendly and degradable networks. The most common biomass precursors suitable for the preparation of biopolymers are cellulose, starch, proteins, and lipids.[3,5–7]

Biomass is an abundant renewable resource, and the most abundant source, cellulose, provides access to valuable compounds through pyrolysis.[8] Levoglucosenone (LGO) is a bicyclic compound obtained from the pyrolysis of cellulose and is a desirable chiral molecule for the synthesis of green solvents, natural products, therapeutic agents and molecules with fixed and known stereochemistry.[8–11] The Circa group has developed a catalytic aerobic fast pyrolysis method for the bulk production of LGO from waste biomass.[10] They have reported the capacity to produce LGO on an industrial scale (50 tons per year) and its derivative Cyrene™ is a bio-based solvent that is an alternative to hazardous dipolar aprotic solvents.[12,13] Due to possessing several unique structural features and being accessible on an industrial scale, LGO is becoming increasingly popular in various research fields.[14,15] It is an unsaturated bicyclic ketone–diether molecule containing two stereogenic centres. The 1,6-anhydro bridge confines the pyranose ring in the specific conformation and offers excellent facial selectivity. Therefore, it is an ideal candidate for the synthesis of targeted compounds using various reaction pathways.[12,16]

The incorporation of LGO into traditional step-growth polymers such as polyesters, polyamides, and polyurethanes is

[a]*School of Natural Sciences-Chemistry, University of Tasmania, Hobart, Tasmania 7005, Australia. E-mail: stuart.thickett@utas.edu.au*
[b]*School of Engineering, Royal Melbourne Institute of Technology, Melbourne, Victoria, 3000, Australia*

† Electronic supplementary information (ESI) available. See DOI: https://doi.org/10.1039/d5py00339c

potentially an interesting method for the synthesis of novel biodegradable and environmentally friendly materials.[17–19] These materials have applications in biomedical goods and numerous other sectors including food packaging.[17,20] In recent work, researchers have leveraged LGO to synthesize renewable biopolymers as an alternative to non-renewable polymers using various polymerization techniques such as ring-opening metathesis polymerization (ROMP), cationic ring-opening polymerization (CROP) and thiol–ene chemistry.[9,21–23]

In recent years, thiol–ene "click" chemistry has become popular with various bio-based platforms including levoglucosan,[21,24] levoglucosenone,[9,22] isosorbide,[25,26] furan[27] and terpene[25,28] derivatives to generate both linear and network polymers. This is in part due to its rapid reaction kinetics, and potential to achieve quantitative conversion involving a stereospecific and orthogonal equimolar reaction between thiol and alkene functionalities. Additionally, the reaction is oxygen-tolerant during curing.[29] The resulting network polymers have low shrinkage, possess a homogenous structure and overall are considered a more environmentally friendly technique.[30–33] This was recently demonstrated by Flourat *et al.*[34] who took advantage of this thiol–ene photopolymerization technique in LGO chemistry to obtain bio-based and more eco-friendly thermosets with T_g ranging from −8 to 11 °C depending on the carbon chain length in the monomers.

Our research group has recently focused on the synthesis of polymers having a high fraction of bio-derived carbon. There is an abundance of reports demonstrating the synthesis of various biobased compounds using fatty acids and plant-based acids. Hernández *et al.*[35] have worked on bio-based polymers obtained from modified fatty acids. They used oleic acid and lauric acid, converting them into ester derivatives. Inspired by this research we were successfully able to prepare LGO-based ester derivatives using unsaturated fatty acids such as oleic acid and linoleic acids. Similarly, plant-based unsaturated acids such as 10-undecenoic acid and citronellic acid were linked with levoglucosenol (**HO-LGO**) through ester linkage based on the study of Döpping *et al.*[36] These monomers synthesized from fatty acids and plant-based acids assisted in improving the biobased carbon up to two times in the corresponding polymer than in our previous work which used allyl ether and pentenoic acid ester derivatives of LGO.[22] Furthermore, we were interested in investigating the potential of LGO-derived carbamates, similar to the work performed by Goculdas *et al.*[37] After the successful synthesis of carbamates we turned our attention to the focus on obtaining carbonates using allyl alcohol and 4-pentenol with **HO-LGO**. The carbamate and carbonate monomers extended the class of polymers that have been presented in the literature, providing access to unique mechanical properties.

Expanding on our previous study,[22] herein we utilize the reduced form of LGO *i.e.*, **HO-LGO**, to develop the synthesis of seven novel bio-based diene monomers suitable for thiol–ene photopolymerization. These monomers contain the inherent double bond inside the bicyclic system and a double bond added through LGO derivatization. During monomer synthesis, we varied the carbon chain length from three to eighteen in addition to changing the linking functional groups (such as ester, carbonate and carbamate) to tune the material properties. Initially, we focused on linking fatty acids (oleic and linoleic acid) and plant-derived acids (citronellic and 10-undecenoic acid) to form esters and then some carbonates and carbamate leveraging the hydroxy group of **HO-LGO**. As per our previous approach,[22] all the monomers were subsequently polymerized *via* thiol–ene "click" chemistry utilizing commercially available tetra-thiol to generate cross-linked networks. The polymerization kinetics were studied using real-time FTIR, and the thermal and mechanical properties of the networks were shown to be strongly dependent on monomer structure. The hydrolytic degradation of the networks was analysed in an alkaline medium, to demonstrate the potential of these materials for chemical degradation under relatively benign conditions.

Experimental

Materials

All reagents and solvents such as 10-undecenoic acid, citronellic acid, oleic acid, linoleic acid, allyl chloroformate, 4-penten-1-ol, allylamine, 1,1′-carbonyldiimidazole (CDI), 4-dimethylaminopyridine (DMAP), dichloromethane (DCM), ethyl acetate (EtOAc), *n*-hexane, and pyridine used in these studies were used as received from Sigma-Aldrich, AK Scientific, Combi-Blocks, and Oakwood. Other commercially available reagents such as acids bases and salts from these vendors were used without further purification. LGO was received from Circa group. TLC was performed using Merck silica gel 60-F254 plates. Developed TLC plates were visualized by using UV light and potassium permanganate stain ($KMnO_4$, K_2CO_3, H_2O). Automated flash column chromatography was conducted with a Reveleris® X2 flash chromatography system with 12 and 40 μm silica gel cartridges. Unless otherwise specified, reactions were conducted with magnetic stirring under nitrogen.

Characterization

NMR spectroscopic experiments were performed on a Bruker Avance III NMR spectrometer operating at 600 MHz (^{1}H) or 150 MHz (^{13}C). The deuterated solvents used were $CDCl_3$ and D_2O. Chemical shifts were recorded in ppm. Spectra were calibrated by assignment of the residual solvent peak to δ_H = 7.24 ppm and δ_C = 77.23 ppm for $CDCl_3$ and δ_H = 4.80 ppm for D_2O. Coupling constants (J) were recorded in Hz. Molecular mass was analysed by infusion into an Orbitrap Q-Exactive HF mass spectrometer equipped with a heated electrospray ionization (HESI) source. Data were acquired over the scan range of 150–2000 m/z in positive ionization mode at a resolution of 240 000 K.

FTIR was performed on a Bruker Vertex 70 FTIR spectrometer using a Bruker platinum ATR accessory with a diamond crystal and a liquid-nitrogen-cooled MCT detector. Spectra

were recorded in the range of 4000–600 cm^{-1}. 32 scans were used for the background and sample measurement. A UV lamp (370 nm, 54 W sun UV led nail lamp) was used during the polymerization and polymerization kinetics study.

Dynamic mechanical analysis (DMA) of cured specimens was performed using single cantilever mode on a TA Q800 dynamic mechanical analyser. Specimens were cured in a mold with dimensions length × width × thickness = 17 × 8 × 2 mm. The actual dimensions were measured with a digital calliper. The experimental method was as follows: from −15 °C to 100 °C at 2 °C min^{-1} (3 °C min^{-1} for samples 1–3). A constant frequency of 1 Hz and displacement of 5 μm was use. DMA measurements were performed in duplicate. The glass transition temperature was determined using the temperature at the peak of the tan δ curve. The cross-linking density ν was determined *via* eqn (1) below:

$$\nu = \frac{E'}{3RT} \quad (1)$$

where R is the universal gas constant, T the absolute temperature at a value 30 K above the peak in the tan δ curve, and E' is the storage modulus at this temperature.

A 100 kN Instron mechanical tester with a tensile grip fixture was used to measure the tensile test of cured polymer samples. For tensile samples, the dog-bone tabbed ends were used. Differential scanning calorimetry (DSC) experiments were performed using a Netzsch Caliris 300 instrument. The samples were encapsulated into an aluminium crucible during sample preparation. A temperature range from −25 °C to 100 °C was used to monitor thermal transition. Three loops of heating and cooling were performed, and a second heating loop was taken to determine the T_g results. The standard heating rate of 10 °C per minute was applied during analysis. Thermogravimetric analysis (TGA) was performed using a Netzsch STA 449 F5 Jupiter. Aluminium oxide crucibles were used to hold the sample in the furnace. The sample (~15 mg) was heated from 25 to 800 °C at a rate of 10 °C per minute in a high-purity nitrogen atmosphere. The contact angle was measured at room temperature using a smart Surface Electro Optics Phoenix equipped with a 22-gauge needle. Approximately 3.50 μL deionized water droplet was placed on the smooth surface of clean polymer samples. The final contact angle for each sample was calculated as the average of three measurements.

Synthesis of HO-LGO

HO-LGO was synthesized by using Ma and coworkers' method.[38] LGO (5 g, 39.65 mmol) was dissolved in methanol (60 mL) and cooled at 0 °C. The solution was then treated carefully with $CeCl_3{\cdot}7H_2O$ (15.0 g, 40.25 mmol, 1 equiv.) and $NaBH_4$ (1.5 g, 36.95 mmol, 1 equiv.). After stirring for 1 h, the solvent was evaporated, and the residue was subjected to flash chromatography (2 : 1 v/v ethyl acetate/hexane elution) to afford the allylic alcohol (**HO-LGO**) as a white crystalline solid in 91% yield.

Synthesis of monomer 1

10-Undecenoic acid (7.0 g, 37.99 mmol, 1 equiv.) was dissolved in dry dichloromethane (DCM) (60 mL). 1,1′-Carbonyldiimidazole (CDI) (8.0 g, 49.38 mmol, 1.3 equiv.) was added and stirred at room temperature for 2 h to form the intermediate compound ***a*** (see Scheme 1). The formation of the intermediate was monitored by TLC and ^{1}H NMR. **HO-LGO** (3.75 g, 29.27 mmol, 1 equiv.) and 4-dimethylaminopyridine (DMAP) (0.36 g, 2.93 mmol, 0.1 equiv.) were added to the flask containing the intermediate compound and the reaction mixture refluxed for 12 h. Water (60 mL) was added, and the mixture was extracted with DCM (3 × 60 mL). The organic phase was dried and evaporated to give the product which was purified by column chromatography to obtain the monomer **1** as a colourless oily liquid (6.25 g, 21.24 mmol, 73% yield), R_f 0.79 (EtOAc–hexane, 2 : 3 v/v).

Synthesis of monomer 2

Citronellic acid (4.7 g, 28.12 mmol, 1 equiv.) was dissolved in dry DCM (60 mL). CDI (6.24 g, 36.55 mmol, 1.3 equiv.) was slowly added and stirred at room temperature for 2 h. Water (60 mL) was added, and the mixture was extracted with DCM (3 × 60 mL). The organic phase was dried and evaporated to obtain the intermediate product ***b***. **HO-LGO** (3.64 g, 28.39 mmol, 1 equiv.) was dissolved in DCM (60 mL); the intermediate compound ***b*** obtained in the previous step and DMAP (0.35 g, 2.84 mmol, 0.1 equiv.) was added and the reaction mixture refluxed for 12 h. Water (60 mL) was added, and the mixture was extracted with DCM (3 × 60 mL). The organic phase was dried and evaporated to give the product which was purified by column chromatography to obtain monomer **2** as a colourless oily liquid (5.98 g, 21.34 mmol, 76% yield), R_f 0.31 (EtOAc–hexane, 1 : 9 v/v).

Synthesis of monomer 3

Oleic acid (7.0 g, 24.78 mmol) was dissolved in dry DCM (60 mL), and CDI (5.49 g, 32.04 mmol, 1.3 equiv.) was added and stirred at room temperature for 3 h. Water (60 mL) was added, and the mixture was extracted with DCM (3 × 60 mL). The organic phase was dried and evaporated to obtain the intermediate product ***c***. **HO-LGO** (3.0 g, 23.42 mmol, 1 equiv.) was dissolved in DCM (60 mL) and the intermediate compound ***c*** and DMAP (0.29 g, 2.34 mmol, 0.1 equiv.) were both added and the reaction mixture refluxed for 12 h. Water (60 mL) was added, and the mixture was extracted with DCM (3 × 60 mL). The organic phase was dried and evaporated to give the product which was purified by column chromatography to obtain the monomer **3** as a colourless oil (7.82 g, 19.93 mmol, 86% yield), R_f 0.56 (EtOAc–hexane, 1 : 4 v/v).

Synthesis of monomer 4

Linoleic acid (0.5 g, 1.78 mmol) was dissolved in dry DCM (10 mL), and CDI (0.4 g, 2.32 mmol, 1.3 equiv.) was added and stirred at room temperature for 3 h. Water (20 mL) was added, and the mixture was extracted with DCM (3 × 20 mL). The

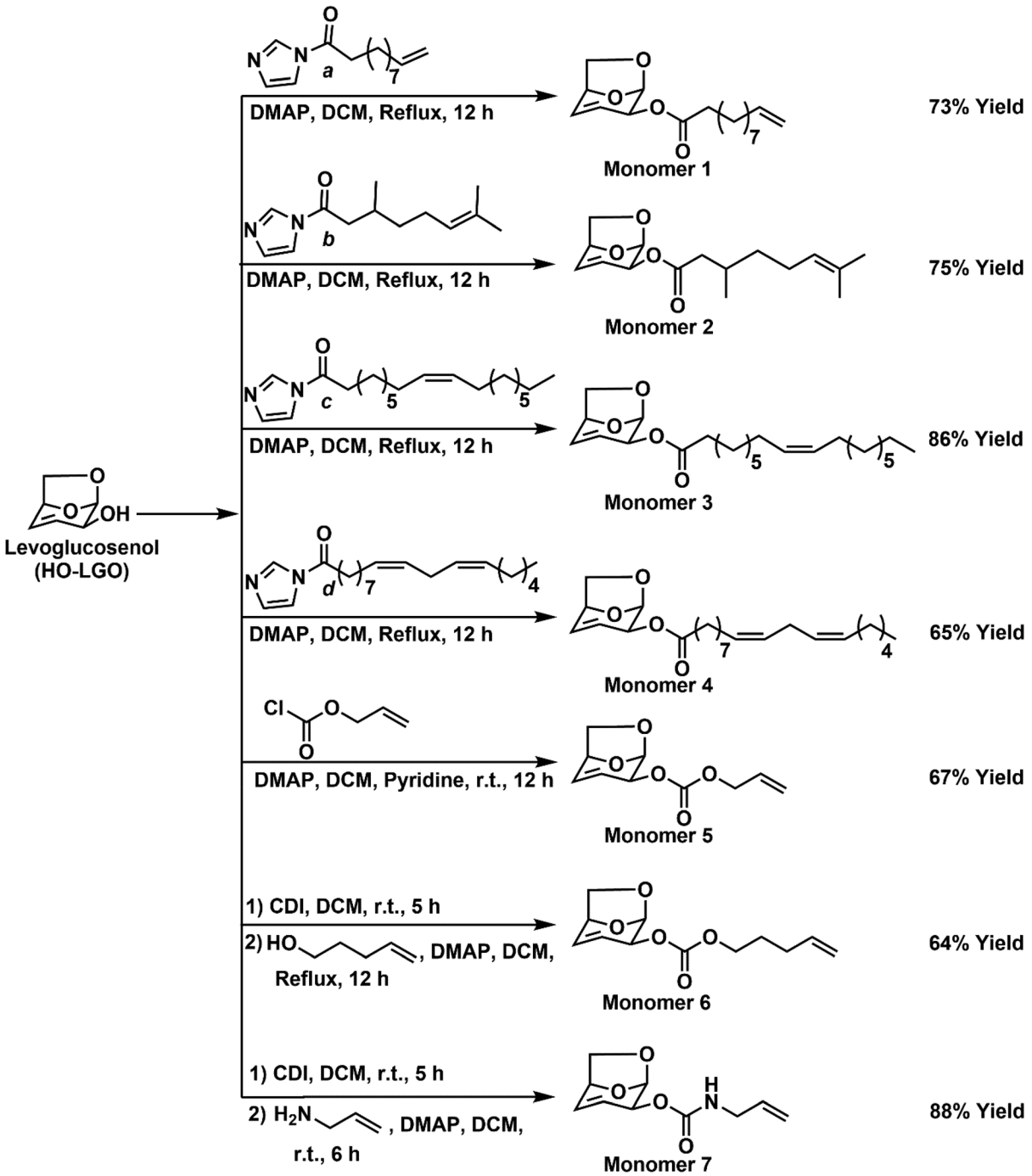

Scheme 1 Synthesis of monomers **1** to **7** from **HO-LGO**.

organic phase was dried and evaporated to obtain the intermediate product ***d***. **HO-LGO** (0.2 g, 1.54 mmol, 1 equiv.) was dissolved in DCM (10 mL) and the intermediate compound ***d*** and DMAP (0.02 g, 0.15 mmol, 0.1 equiv.) were both added and the reaction mixture refluxed for 12 h. Water (20 mL) was added, and the mixture was extracted with DCM (3 × 20 mL). The organic phase was dried and evaporated to give the product which was purified by column chromatography to obtain the monomer **4** as a colourless oil (0.39 g, 1.01 mmol, 65% yield), R_f 0.56 (EtOAc–hexane, 1 : 4 v/v).

Synthesis of monomer 5

HO-LGO (5.0 g, 39.03 mmol) was dissolved in dry DCM (60 mL) and allyl chloroformate (6.30 g, 50.73 mmol, 1.3 equiv.), DMAP (0.48 g, 3.90 mmol, 0.1 equiv.) and pyridine (15.43 g, 195.13 mmol, 5 equiv.) were added. The reaction

mixture was stirred at room temperature for 12 h. The crude product was initially washed with 2 M HCl (60 mL) and finally with 2 M Na_2CO_3 (60 mL). The organic extract was evaporated and dried to give the crude product that was purified by column chromatography (EtOAc/hexane) to obtain monomer **5** as a colourless oil (5.53 g, 26.06 mmol, 67% yield), R_f 0.63 (EtOAc–hexane, 2 : 3 v/v).

Synthesis of monomer 6

HO-LGO (0.1 g, 0.78 mmol, 1 equiv.) was dissolved in dry DCM (6 mL), and CDI (0.17 g, 1.01 mmol, 1.3 equiv.) was slowly added and stirred at room temperature for 5 h. Water (20 mL) was added, and the mixture was extracted with DCM (3 × 20 mL). The organic phase was dried and evaporated to obtain the intermediate product. 4-Penten-1-ol (0.07 g, 1.01 mmol, 1.1 equiv.) was dissolved in DCM (8 mL) and the intermediate compound and DMAP (0.01 g, 0.08 mmol, 0.1 equiv.) were both added, and the reaction mixture refluxed for 12 h. Water (20 mL) was added, and the mixture was extracted with DCM (3 × 20 mL). The organic phase was dried and evaporated to give the product which was purified by column chromatography to obtain the monomer **6** as a colourless oil (0.12 g, 0.45 mmol, 64% yield), R_f 0.35 (EtOAc–hexane, 1 : 4 v/v).

Synthesis of monomer 7

HO-LGO (5.0 g, 39.02 mmol, 1 equiv.) was dissolved in dry DCM (60 mL), CDI (8.66 g, 50.73 mmol, 1.3 equiv.) was added slowly and stirred at room temperature for 5 h to obtain an intermediate compound (monitored by TLC and ^{1}H NMR). The flask containing the intermediate was treated with allyl amine (3.41 g, 58.55 mmol, 1.5 equiv.) in the presence of DMAP (0.48 g, 3.90 mmol, 0.1 equiv.) and the reaction mixture stirred at rt for 12 h. Water (60 mL) was added, and the mixture was extracted with DCM (3 × 60 mL). The organic phase was dried and evaporated to give the product which was purified by column chromatography to obtain the monomer **7** as a slightly pale-yellow oil (7.21 g, 34.14 mmol, 88% yield), R_f 0.47 (EtOAc–hexane, 2 : 3 v/v).

General procedure for polymerizations

In a typical experiment, the diene monomer (2 equiv.) was mixed with the pentaerythritol tetrakis(3-mercaptopropionate) (tetra-thiol) (1 equiv., denoted 4SH) in an aluminium foil-wrapped vile and mixed properly using a magnetic stirrer. DPO (0.2% w/w) was added to the reaction mixture and stirred/sonicated at room temperature to mix them homogeneously. The mixture was transferred to the dog-bone-shaped mold and cured with UV light (370 nm, 54 W sun UV led nail lamp).

General procedure of degradation

Four polymer samples were added in separate vials containing 1 M NaOH at room temperature and monitored the weight loss in 24 h interval. Once the degradation was completed, the degraded products were divided into two halves. One half of the degraded solution remained as an aqueous basic solution, and the other half was acidified with 1 M HCl and subsequently extracted using ethyl acetate. Both the ethyl acetate extract and the aqueous phase were analysed *via* ^{1}H NMR, ^{13}C NMR and FTIR spectroscopy. In addition, the acidified extract of the poly(3-*co*-4SH) and poly(7-*co*-4SH) were further purified for the detail analysis of degraded fragments.

Results and discussion

Synthesis of monomers and their characterization

In this work, several multifunctional monomers were prepared using both LGO and several naturally occurring unsaturated compounds, such as 10-undecenoic, citronellic, oleic and linoleic acid. 10-Undecenoic acid is a monounsaturated acid derived from castor oil[36] while citronellic acid is a medium-chain monounsaturated fatty acid primarily found in essential oils of *Pelargonium* species at levels ranging from 27.9 to 89.3% (%w/w).[39] Similarly, long-chain unsaturated fatty acids such as oleic and linoleic acids are abundant in olive oil (55–83% w/w)[40] and soybean oil (55% w/w)[41] respectively. These compounds were reacted with **HO-LGO** as described in Scheme 1 (monomers **1–4**) to prepare diene or triene-type monomers that comprise the rigid **HO-LGO** bicyclic ring and an unsaturated, bio-derived side chain connected *via* an ester linkage. Two monomers with carbonate linkage (monomers **5** and **6**) and a carbamate (monomer **7**) were also prepared with a view towards modifying the properties of the resulting polymers through the differing chemistries of the linker unit. **HO-LGO** was obtained by the reduction of LGO using the method of Ma and co-workers (91% yield).[38] To prepare monomers with ester functionality, we used a method similar to our previous approach,[22] where initially – *N*-acyl imidazole intermediates ***a***, ***b***, ***c*** and ***d*** were prepared by the reaction of 10-undecenoic acid, citronellic acid, and two unsaturated fatty acids (oleic acid and linoleic acid) with CDI respectively. The ^{1}H NMR of these monomers are shown in, Fig. S29–S32 of the ESI.† **HO-LGO** and DMAP were subsequently added to these intermediates and refluxed in DCM for 12 h, to obtain monomers **1**, **2**, **3** and **4** in good yields (see Scheme 1). Confirmation of the monomer structures was supported *via* 1D and 2D NMR (see Fig. S1–S16 of the ESI†) analysis, as well as mass spectrometry (see Fig. S34–S37 of the ESI†). Monomers **1–4** consist of 100% bio-derived carbon (see Table 1).

Under the same catalytic and solvent conditions as the ester-based monomers, a carbonate-based monomer (monomer **5**) was successfully prepared by the reaction of allyl chloroformate with **HO-LGO** at room temperature obtaining a 67% yield. An additional carbonate **6** was prepared as well as a carbamate **7**, however, a different synthetic methodology was employed. For the synthesis of monomers **6** and **7**, **HO-LGO** was initially converted into *N*-acyloxy imidazole intermediate (^{1}H NMR spectra can be found in Fig. S33, ESI†) through reaction with CDI. This intermediate was reacted with 4-penten-1-ol or allyl amine in the presence of a DMAP catalyst to obtain carbonate **6** (64% yield) and carbamate **7** (88% yield) (Scheme 1). Monomer **6** was obtained after reflux of the reac-

Table 1 Preparation of polymer from each monomer and calculation of bio-based carbon content for each thiol network

Monomer	Polymer code	No. of carbon atoms per diene	No. of bio-based carbon per diene	No. of carbon atoms per tetra-thiol	Total carbon atoms (2 : 1 diene : tetra-thiol)	Bio-based carbon per thiol–ene network (%)
1	Poly(1-*co*-4SH)	17	17	17	51	66.7
2	Poly(2-*co*-4SH)	16	16	17	49	65.3
3	Poly(3-*co*-4SH)	24	24	17	65	73.8
5	Poly(5-*co*-4SH)	10	6	17	37	32.4
6	Poly(6-*co*-4SH)	12	6	17	41	29.3
7	Poly(7-*co*-4SH)	10	6	17	37	32.4

tion mixture in DCM for 12 h, whereas synthesis of monomer **7** was possible within 6 h at room temperature. The ^{1}H and ^{13}C NMR of monomers **5–7** are shown in Fig. S17, S18, S21, S22, S25 and S26, ESI.† These structures were also supported by mass spectrometry (see Fig. S38–S40, ESI†). Monomers **5–7** have a lower percentage of bio-derived carbon than monomers **1–4**, however, the variation in functional linker gives significantly different thermal and mechanical properties in the resulting polymer networks (see subsequent discussion). We have thus developed a catalogue of **HO-LGO**-derived monomers with high levels of bio-derived carbon possessing ester, carbonate and carbamate linkers whilst preserving the internal double bond of the **HO-LGO** for subsequent polymerization.

Thiol–ene photopolymerization and kinetic study of bio-based networks

The dienes and one triene (monomer **4**) prepared in this work were subsequently polymerized using thiol–ene "click" chemistry to prepare cross-linked polymeric thermosets (Fig. 1). A commercially available tetra-thiol (denoted 4SH) was mixed with the desired monomer along with a UV-active type I photoinitiator in a vial at a concentration of 0.2% w/w; the composition of the mixture was controlled using stoichiometric equivalents of thiol and ene groups. The mixture was then cured in silicone molds by irradiation with UV light (using a 370 nm, 54 W sun UV led nail lamp).

Polymerization kinetics were monitored by analysing the decrease in absorbance corresponding to both the "ene" (1645 cm^{-1} and 3074 cm^{-1}) and thiol (2570 cm^{-1}) functional groups *via* FTIR spectroscopy, to determine functional group conversion in each thermoset. This was achieved by collecting FTIR spectra at 10 s intervals upon continual UV irradiation of the thiol–ene mixture. We have previously shown[22] using model UV photocuring reactions with 1-dodecanethiol that the C=C double bond within the LGO ring is slightly slower to react than terminal C=C bonds in our monomers, however both are fully consumed within 60–120 s of irradiation. Here,

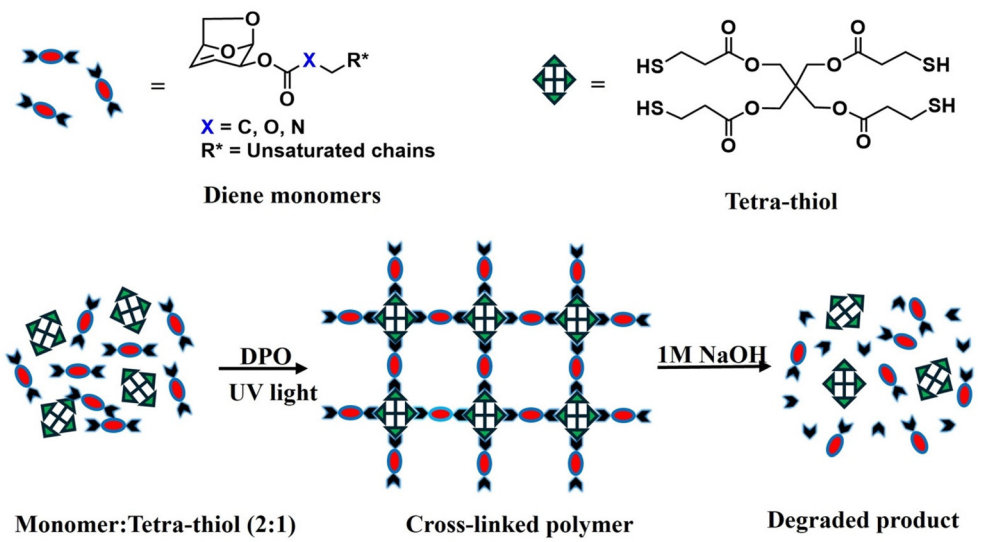

Fig. 1 Schematic illustration of polymerization using thiol–ene chemistry and degradation in an alkaline medium.

based on percentage conversion on thiol–ene photopolymerization of LGO-based monomers, the photocuring was rapid and a solid thermoset was formed in less than one minute for monomers **1**, **2**, **5**, **6** and **7** (see Fig. 2). Near-quantitative conversion of C=C groups was achieved in ~10 s for monomers **1**, **5** and **6**, and ~30 s for monomer **7**. Monomers **2** and **3** were the slowest to polymerize, taking over 60 s to achieve high conversion of ene groups, and the polymer derived from monomer **3** was soft and tacky under these conditions. In order to ensure full polymerization, monomer **3** was polymerized at a higher loading of photoinitiator (0.5% w/w) compared to all other systems (0.2% w/w). The extent of functional group conversion of all six thermosets at t = 0 and at t = 120 s are provided in the ESI (Fig. S47–S52†). The cured thermosets were transparent and colourless (Fig. S62†) in appearance except for the polymer obtained from monomer **7** which possessed a slightly pale-yellow colour.

We note that our attempt to polymerize monomer **4** was unsuccessful under equivalent conditions successfully used for other monomers (Fig. S53 and S54†). The bis-allylic C–H bond in the unsaturated chain within monomer **4** is relatively weak (possessing a bond dissociation energy ~80 kcal mol^{-1}) in comparison to the allylic C–H bonds (88 kcal mol^{-1}) within the other monomers. The estimated bond dissociation energy of the bis-allylic proton is lower than the S–H (84 kcal mol^{-1}).[42] Therefore, the bis-allylic hydrogens in the monomer backbone are relatively good hydrogen atom donors. In the presence of a UV-active photoinitiator and tetra-thiol, thiyl radicals would abstract the hydrogen atom from bis allylic system, generating a carbon-centred free radical that is stabilized by conjugation.[42–44] As a result, this yields either slower or no polymerization. Monomer **4** was subsequently omitted from further characterization and mechanical analysis due to these issues faced during its polymerization.

We also observed *via* visual inspection that increasing the carbon chain length within the fatty acid side chain of the monomers resulted in softer polymer networks. For instance, polymers obtained from the ester-linked monomer **1** (eleven terminal carbon chains) and monomer **2** (ten terminal carbon chains) were flexible. In contrast, monomer **3** which has eighteen carbons on the terminal chain (albeit with a C=C bond in the middle of the chain, generating a nine-carbon branch after polymerization) afforded polymer that was so soft as to be malleable by hand. Monomers **5** and **7** (having only three terminal carbon chains) and monomer **6** (containing two additional carbon atoms in the terminal chain) produced much more rigid networks, as reflected in their mechanical analysis (see next section). These mechanical differences are also in part due to the rigidity and potential hydrogen bonding of the carbonate and carbamate linkers respectively.

Mechanical and thermal analysis of UV-cured networks

The biobased thermosets prepared in this work were subjected to thermal and mechanical analysis. Mechanical analysis was performed at 25 °C on dog-bone-shaped samples (according to ASTM D638-14) which were UV-cured in silicone molds. The results of these are presented in Table 2 and Fig. 3. Mechanical analysis results showed that there was a significant difference in the tensile strength and Young's moduli across the various networks prepared which we attribute to differing lengths of the alkyl side chains of our monomers in addition to the chemical nature of the linker unit. A wide range of tensile strengths (from 0.51 to 53.98 MPa) and Young's moduli (from 0.62 to 450.80 MPa) were observed, as shown in Fig. 3. We group our thermosets into soft (Fig. 3A) and hard (Fig. 3B) materials based on the very large differences in tensile strength and Young's modulus. The softest samples all possessed long alkyl chains from the fatty acids (in addition to the carbonate poly(6-*co*-4SH)) used in their synthesis; samples poly(1-*co*-4SH), poly(2-*co*-4SH) and poly(3-*co*-4SH) possessed both low tensile strengths (2.62, 1.53 and 0.51 MPa respectively) and Young's moduli (3.13, 0.82 and 0.62 MPa respectively). In contrast, the carbonate (monomer **5**) and carbamate (monomer **7**) networks with only three carbons in the monomer side group possessed much higher tensile strength (47.76 and 53.98 MPa)

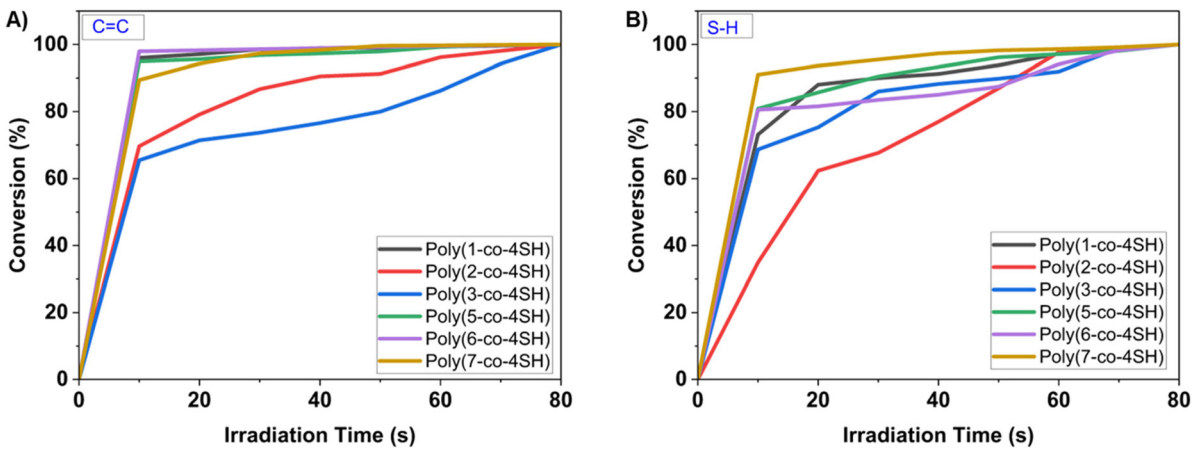

Fig. 2 Percentage conversion *vs.* irradiation time: (A) alkene (C=C) and (B) thiol (S–H), for all six thermosets, based on FTIR analysis during UV irradiation.

Table 2 Thermal and mechanical (tensile) analysis data of our networks

Polymer code	Terminal linker	T_{onset} (°C)	T_{max} (°C)	Residual mass (%)	T_g DSC (°C)	Tensile strength (MPa)	Elongation at break (%)	Young's modulus (MPa)
Poly(1-*co*-4SH)	Ester	359.5	385	2.0	14.4	2.62	83.05	3.13
Poly(2-*co*-4SH)	Ester	334.5	346	1.3	16.2	1.53	186.56	0.82
Poly(3-*co*-4SH)	Ester	350.5	364	2.6	0.3	0.51	85.43	0.62
Poly(5-*co*-4SH)	Carbonate	334.3	365	1.3	37.4	47.76	10.18	450.8
Poly(6-*co*-4SH)	Carbonate	268.4	293	4.1	27.9	12.06	164.71	7.61
Poly(7-*co*-4SH)	Carbamate	309.4	332	9.1	34.1	53.98	13.88	402.54

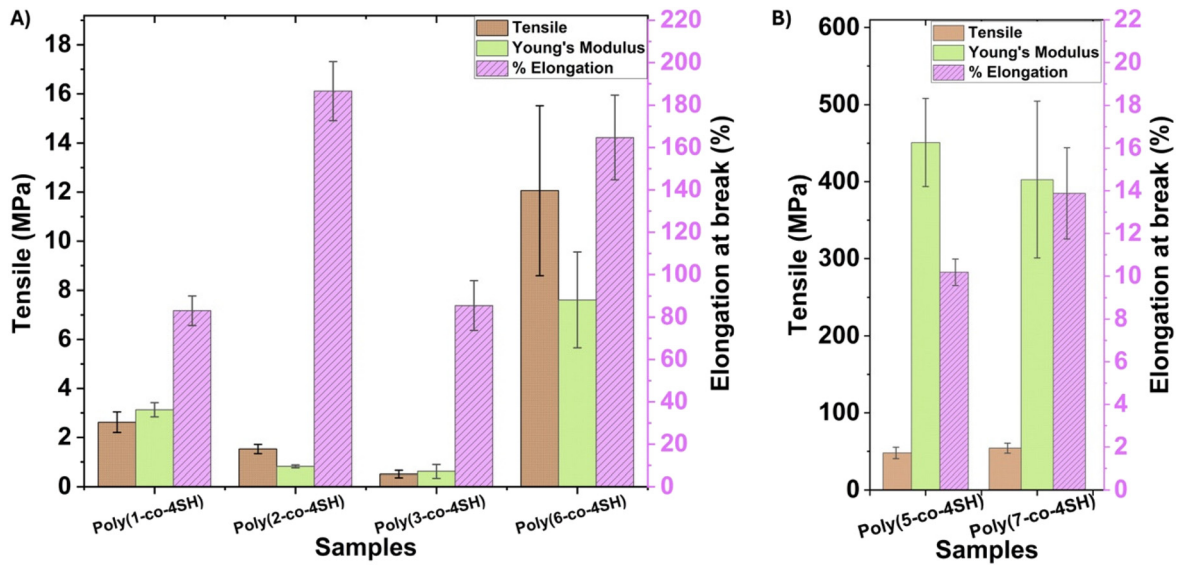

Fig. 3 Mechanical analysis of LGO-based thiol–ene networks: (A) soft polymers and (B) firm polymers (error bars indicate the standard deviation, left *Y*-axis represents tensile strength and Young's modulus and right *Y*-axis represents % elongation at break).

and Young's moduli (450.80 and 402.54 MPa) as observed in Fig. 3B. The softer samples typically demonstrated a larger elongation at break compared to their more rigid counterparts, with a maximum elongation at break achieved for the polymer based on citronellic acid, reaching 186.6%. An interesting comparison exists between the networks prepared from monomers **5** and **6**, which are both carbonates that differ only in an extra two carbons in the pendant side group. Increasing the alkyl pendant by two carbons increases the elongation at break (from 10.2% to 164.7%) of the network, whilst decreasing the tensile strength (from 47.76 to 12.06 MPa) and Young's modulus (from 450.80 to 7.61 MPa), highlighting the tuneability of our network design.

TGA and DSC were used to analyse both the thermal stability and thermal transitions of the cured thermosets. Fig. 4A and B illustrate the mass loss of each thermoset as a function of temperature, and the derivative of this mass loss. All networks have decomposition onset temperatures greater than 250 °C, with five of the six networks possessing a two-step decomposition process; the poly(6-*co*-4SH) network has the lowest decomposition temperature (T_{onset} = 268 °C) along with a three-step mass loss curve. The first prominent mass loss step is attributed to the decomposition of the C–S bond of the resin, and the breaking of the O–C bonds, as previously reported.[22] The third mass loss is attributed to the decomposition of the C–C bond within the network.[9]

The glass transition temperature (T_g) of the six thermosets was determined using DSC (Fig. 4C and Table 2). Unsurprisingly, poly(3-*co*-4SH) had the lowest T_g value of 0.3 °C, which was attributed to the long fatty acid chain present within the monomer structure. When comparing the ester-containing polymers, the sample derived from the longest chain fatty acid monomer (poly(3-*co*-4SH)), possessed a lower T_g than the polymers of shorter carbon chain monomers (poly(1-*co*-4SH) and poly(2-*co*-4SH)). The 9-carbon short chain branch due to the structure of monomer **3** also is likely

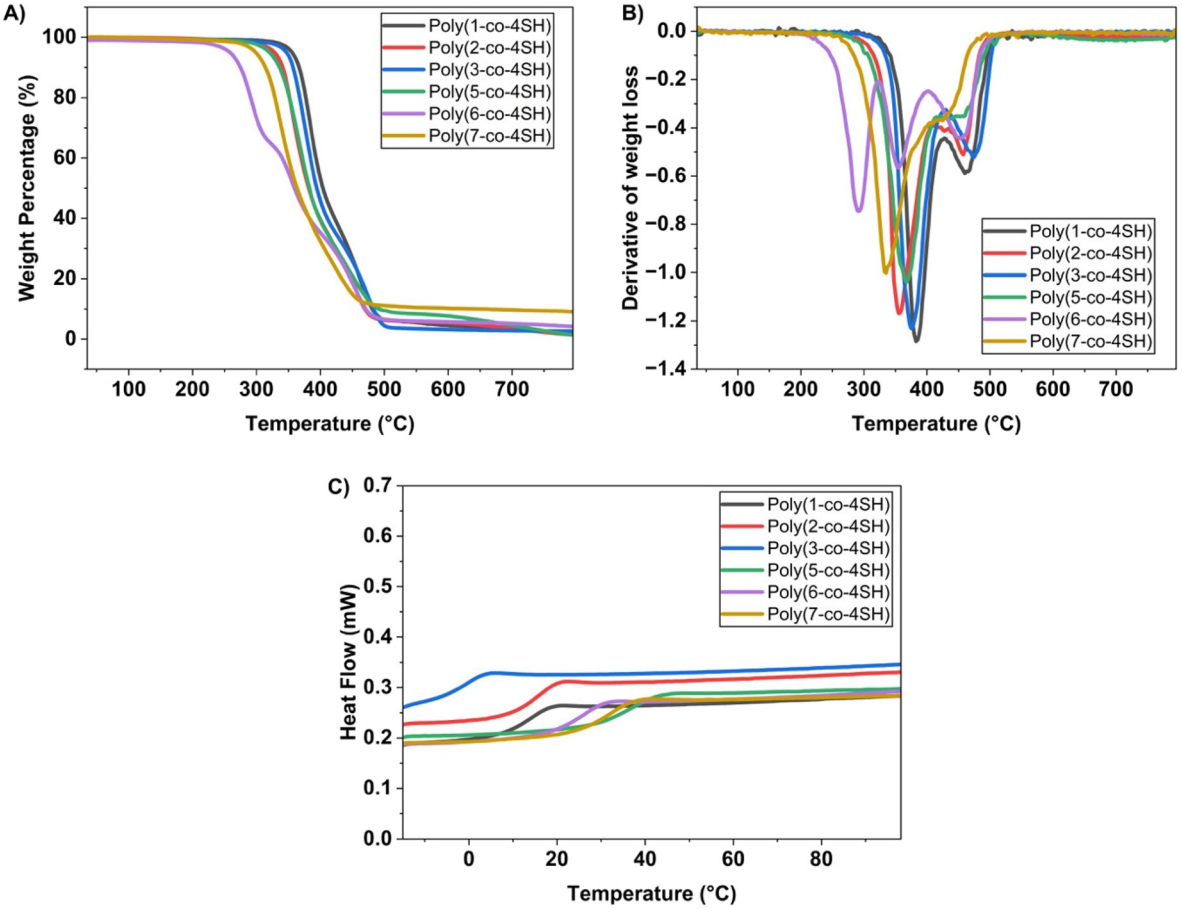

Fig. 4 (A) Percentage of weight loss over the temperature of LGO-based thiol–ene networks. (B) First derivative obtained from the TGA curve. (C) DSC thermograms of all six polymers.

to contribute to the low T_g of this material. Carbonate and carbamate-based monomers possessed the highest glass transition temperature values, with the highest T_g (37.4 °C) belonging to the carbonate with the shortest side chain poly(5-*co*-4SH) (see Table 2). Once again within our two carbonate monomer networks, we observe a trend of decreasing T_g with increasing chain length of the alkyl side chain (*e.g.*, poly(6-*co*-4SH) *vs.* poly(5-*co*-4SH)). We conclude that both the thermal and mechanical performance of our polymer networks are influenced by the targeted design of our bio-based monomers, with the ability to control the mechanical performance and glass transition temperature of the resulting materials.

Dynamic mechanical analysis (DMA) was also performed to study the temperature dependent nature of the storage (E') and loss (E'') moduli of our thermosets, and in addition to determining the cross-linking density within the polymeric structure. The storage modulus (E') and tan delta (defined as the ratio of E''/E') of our thermosets as a function of temperature are shown in Fig. 5 (loss moduli data is shown in Fig. S61, ESI†). We observe a wide range of E' values at ambient conditions (25 °C); poly(1-*co*-4SH), poly(2-*co*-4SH) and poly(3-*co*-4SH) all possess very low E' values (<30 MPa) whereas poly(5-*co*-4SH), poly(6-*co*-4SH) and poly(7-*co*-4SH) all have E' values >1.7 GPa; this trend is identical to the Young's moduli and tensile strength data for our polymers in Table 2. The glass transition temperature by DMA, defined as the maximum in the tan delta curve, show a comparable trend to those measured by DSC (see Table 3), with polymers poly(5-*co*-4SH), poly(6-*co*-4SH) and poly(7-*co*-4SH) all possessing T_g values above room temperature; the other polymers were softer and had T_g values either at or lower than room temperature. The T_g values determined by DMA were systematically higher than those measured by DSC (Table 2); other methods of determining the T_g by DMA (for example, the temperature at which E'' reaches a maximum value, Table S2†) also give an identical trend to our DSC results.

The storage moduli at a temperature 30 K above T_g was used to determine the cross-linking density of our thermosets (see eqn (1) and Table 3). We observed that despite vastly different E', Young's moduli, tensile strength and T_g values, the cross-linking densities were very similar for most thermosets (with values typically between 0.40–0.60 mmol cm^{-3}). This is somewhat unsurprising, given stoichiometric ratios of thiol to ene groups were used for all thermosets. Two exceptions were the oleic ester poly(3-*co*-4SH) and carbamate poly(7-*co*-4SH), which had higher cross-linking densities at 1.26 and

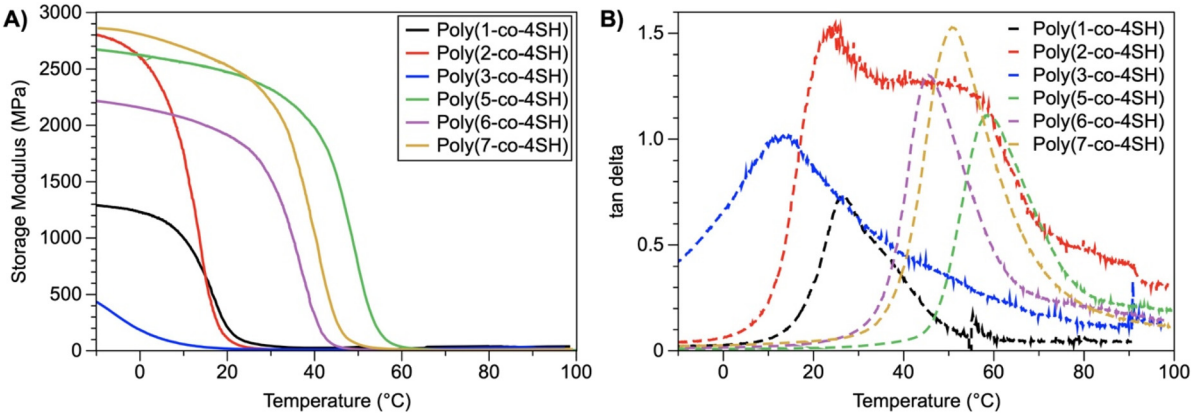

Fig. 5 DMA analysis of UV-cured thermosets, showing both (A) storage modulus and (B) tan delta as a function of temperature.

Table 3 DMA characterization of UV-cured thermosets

Polymer code	E' (MPa) at 25 °C	T_g [a] DMA (°C)	E' (MPa) at (T_g +30) °C	ν [b] (mmol cm^{-3})
Poly(1-*co*-4SH)	10.16	23.7	4.29	0.52
Poly(2-*co*-4SH)	28.07	25.3	3.51	0.42
Poly(3-*co*-4SH)	13.26	13.1	9.98	1.26
Poly(5-*co*-4SH)	2409.7	58.6	5.04	0.55
Poly(6-*co*-4SH)	1787.7	46.8	3.59	0.41
Poly(7-*co*-4SH)	2414.9	52.3	9.53	1.07

[a] Based on the temperature at which tan δ is at its maximum value. [b] As determined from eqn (1) (see Experimental section).

1.07 mmol cm^{-3} respectively. The variation in cross-linking density is a likely factor in the rate of chemical degradation of our poly(3-*co*-4SH) sample, however the hydrophobicity of the material is also important (see later discussion). The cross-linking density could be intentionally varied if desired through changing the ratio of thiol to ene groups prior to photocuring.

Based on the mechanical properties of our thermosets presented here, they have the potential to serve as an alternative to commonly used fossil-fuel-based polymeric materials. Specifically, thermosets poly(1-*co*-4SH), poly(2-*co*-4SH), poly(3-*co*-4SH) and poly(6-*co*-4SH) which exhibit low T_g, greater elongation at break and low tensile strength, and so could potentially serve as substitutes for flexible polymers such as low-density polyethylene (LDPE), silicone elastomers, ethylene vinyl acetate (EVA), plasticized polyvinyl chloride (PVC) and soft polymeric gels, which typically have reported tensile strengths between 7–30 MPa and elongation at breaks from 100–600%. Poly(5-*co*-4SH) and poly(7-*co*-4SH) on the other hand are rigid solids with T_g value above room temperature and possess low elongation and high tensile strength; these materials may be suitable alternatives to rigid polymers such as polystyrene (PS), polyethylene terephthalate (PET), polycarbonate (PC) and polylactic acid (PLA) which have typical tensile strength and elongation at break values from 34–75 MPa and 1–100% respectively. Our bio-based thermosets have high optical transparency (see Fig S62, ESI† for digital photographs) and so have potential as protective coatings or barrier products. As a further advantage, our bio-based thermosets can be chemically degraded under relatively mild conditions (see next section).

Chemical degradation of thiol–ene networks

The degradation of the cured networks was studied in an alkaline medium at room temperature. Previous studies have shown that polymers using an ether and ester linkage to introduce the alkene are susceptible to hydrolytic cleavage.[22,45] These polymers also contained ester linkages introduced *via* the tetra-thiol. Herein, networks containing ester, carbonate and carbamate functionality were investigated for their degradation behaviour. Four representative samples (Fig. 6) of the LGO-derived polymer networks were selected and monitored for their degradation in 1 M NaOH solution. These materials do not swell in water, suggesting degradation driven from the surface; the degradation of the poly(7-*co*-4SH) network was rapid (2 days) followed next by poly(5-*co*-4SH) (3 days). The process was significantly slower for the poly(3-*co*-4SH) and poly(6-*co*-4SH) networks, highlighting that targeted monomer design enables tuneable degradation kinetics of the resulting network. The varying rates of degradation are correlated to both the carbon chain length of the side chain within the monomer structure and the functional group present in each network. Due to having a shorter carbon chain along with the N–H group in the poly(7-*co*-4SH) network, it has a more hydrophilic character than the networks containing carbonate and ester functional groups. This is supported by static water contact angle measurements. As expected, poly(7-*co*-4SH)

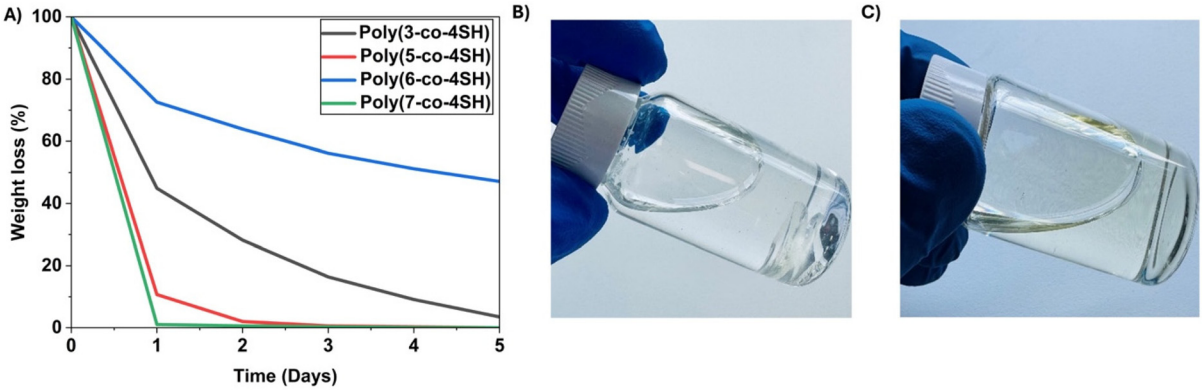

Fig. 6 (A) Degradation study of the poly(3-*co*-4SH), poly(5-*co*-4SH), poly(6-*co*-4SH) and poly(7-*co*-4SH) networks in 1 M NaOH solution. Vials with poly(7-*co*-4SH) polymer: (B) before decomposition and (C) after two days.

exhibited the lowest contact angle (55.9°), while poly(3-*co*-4SH) displayed the highest (67.7°) among these thermosets. Poly(5-*co*-4SH) (63.6°) and poly(6-*co*-4SH) (65.9°) displayed intermediate contact values. All the networks are relatively hydrophilic with static contact angles <90°, even those with fatty side chains such as poly(3-*co*-4SH), which is attributed to the polar nature of the thiol within the network. Network polymers with relatively shorter carbon chains, such as poly(5-*co*-4SH) and poly(7-*co*-4SH), were degraded more quickly than bulkier side groups, with at times quite large effects on degradation (*e.g.* an extra two carbon atoms from poly(6-*co*-4SH) compared to poly (7-*co*-4SH) significantly increased the degradation time). This result (see Table S3†) is aligned with our previous study.[22]

The degradation products of various thermosets in 1 M NaOH were studied *via* ^{1}H and ^{13}C NMR and FTIR spectroscopy to provide insight into the mechanism of polymer degradation. This was achieved *via* acidifying the aqueous solution of degraded products followed by NMR analysis, in addition to ethyl acetate liquid–liquid extraction and purifying the soluble extracts (see Experimental section for further details). In the case of the ester-based poly(3-*co*-4SH), which contains fatty acid chains derived from oleic acid, the major isolated product after ethyl acetate extraction was a substituted oleic acid derivative. The ester linkages of both monomer **3** and PETMP are susceptible to hydrolysis, resulting in a 3-mercaptopropionic acid functionalized oleic acid being recovered as the purified major component (see Fig. S63–S66, ESI†). Signals that suggest a 3-mercaptopropionic acid substituted **HO-LGO** product were observed in the remaining fractions (see Fig. S63, ESI†). These findings support the notion that all ester linkages in both the LGO-based monomer and the PETMP tetra thiol are cleaved *via* base hydrolysis to promote network degradation, which is comparable to other reported degradation studies of thiol–ene thermosets with ester linkages within the structure.[46–48]

We also analysed the degradation of the carbamate-based poly(7-*co*-4SH) network, which showed the most rapid degradation in alkaline solution. A mixture of compounds were identified in both the basic aqueous solution as well as the acidified extract *via* ^{1}H NMR (see Fig. S67–71, ESI†). The crude acidified extract was shown to contain signals arising from 3-mercaptopropionic acid, levoglucosenol (**HO-LGO**), and the sulfide and disulfide of 3-mercaptopropionic acid. Extracts from the basic fraction contained the pentaerithytol core from PETMP, pentaerithryol diacetate ester (as major fraction), and **HO-LGO** as minor fraction. These findings suggest less-than-quantitative conversion of LGO double bonds and thiol groups from PETMP during the formation of this thermoset. Polymeric networks readily form at monomer conversions <100%, and so it is plausible that a small fraction of unreacted alkene and thiol groups exist within the network structure, giving rise to the identified compounds post-degradation. The degradation products of these thermosets can thus be readily identified *via* NMR and FTIR spectroscopy, with the materials showing bond cleavage through the abundant linkages within the structure susceptible to base hydrolysis.

Conclusions

This work expands the library of LGO-derived diene monomers, introducing ester, carbonate and carbamate functionality as linkers to other unsaturated compounds, and their subsequent use in thiol–ene photopolymerization. The monomers containing ester functionality were derived from either fatty acids or plant-based acids, and the structure of the side chains contributed to the thermal and mechanical properties of the resulting thermosets. All thermosets possessed good thermal stability (up to 300 °C) and tuneable glass transition temperature. Carbonates and carbamates based on LGO were also prepared, which typically gave highly rigid structures. The tensile strength and Young's modulus of carbonate poly(5-*co*-4SH) and carbamate poly(7-*co*-4SH) reported here surpass the published mechanical properties of LGO-based polymers in the literature, highlighting the benefit of introducing carbonates and carbamates to bio-based thermosets. The degradation of the cured thermoset networks in an alkaline medium was also shown, revealing the material can be degraded with tuneable kinetics based on the nature of the LGO monomer. Given their

impressive mechanical properties, tuneable thermal properties, rapid curing and high transparency, we believe these materials represent an exciting step forward in the design of bio-derived thermosetting materials based on LGO.

Author contributions

Conceptualization by M. K. S., J. A. S. and S. C. T., data curation by M. P. T., formal analysis by M. P. T., funding acquisition by J. A. S. and S.C.T., investigation by M. P. T., methodology by M. P. T., M. K. S., J. A. S. and S. C. T., resources by J. A. S. and S. C. T., supervision by M. K. S., J. A. S. and S. C. T., validation by M. K. S., J. A. S. and S. C. T., writing (original draft) by M. P. T. and writing (review and edited) by M. K. S., J. A. S. and S. C. T. All authors discussed the results.

Conflicts of interest

The authors declare no conflict of interest.

Data availability

The data that supports all the findings of this study are available in the ESI.† Data includes: $^{1}H/^{13}C$/2D NMR spectra of all monomers and intermediates; mass spectrometry data of all monomers; FTIR spectra of monomers and resulting polymers; stress–strain curves from tensile testing; degradation data (mass *vs*. time) of thermosets in alkaline media; dynamic mechanical analysis data (DMA).

Acknowledgements

MPT thanks the College of Science and Engineering, University of Tasmania for the provision of a Graduate Research Scholarship. MKS, JAS and SCT thank the Department of Education, Skills, and Employment, Australian Government for funding *via* the Regional Research Collaboration Program. SCT acknowledges the Australian Research Council for the provision of a Future Fellowship (FT220100096). All authors thank the Central Science Laboratory, University of Tasmania, for NMR, FTIR and mass spectrometry infrastructure and access, as well as Dr James Horne for assistance. We gratefully acknowledge Nadia Zakhartchouk and the Analytical Chemistry Technical Team at RMIT University Melbourne, for their technical support with dynamic mechanical analysis.

References

1 C. O. Tuck, E. Pérez, I. T. Horváth, R. A. Sheldon and M. Poliakoff, Valorization of Biomass: Deriving More Value from Waste, *Science*, 2012, **337**, 695–699.
2 W. Post, A. Susa, R. Blaauw, K. Molenveld and R. J. I. Knoop, A Review on the Potential and Limitations of Recyclable Thermosets for Structural Applications, *Polym. Rev.*, 2020, **60**, 359–388.
3 L. A. Lucia, Lignocellulosic biomass: A potential feedstock to replace petroleum, *BioResources*, 2008, **3**, 981–982.
4 D. K. A. Barnes, F. Galgani, R. C. Thompson and M. Barlaz, Accumulation and fragmentation of plastic debris in global environments, *Philos. Trans. R. Soc., B*, 2009, **364**, 1985–1998.
5 J. J. Bozell and G. R. Petersen, Technology development for the production of biobased products from biorefinery carbohydrates—the US Department of Energy's "Top 10" revisited, *Green Chem.*, 2010, **12**, 539.
6 F. H. Isikgor and C. R. Becer, Lignocellulosic biomass: a sustainable platform for the production of bio-based chemicals and polymers, *Polym. Chem.*, 2015, **6**, 4497–4559.
7 G. Coppola, M. T. Gaudio, C. G. Lopresto, V. Calabro, S. Curcio and S. Chakraborty, Bioplastic from Renewable Biomass: A Facile Solution for a Greener Environment, *Earth Syst. Environ.*, 2021, **5**, 231–251.
8 M. B. Comba, Y. Tsai, A. M. Sarotti, M. I. Mangione, A. G. Suárez and R. A. Spanevello, Levoglucosenone and Its New Applications: Valorization of Cellulose Residues: Levoglucosenone and Its New Applications: Valorization of Cellulose Residues, *Eur. J. Org. Chem.*, 2018, 590–604.
9 A. L. Flourat, L. Pezzana, S. Belgacem, A. Dosso, M. Sangermano, S. Fadlallah and F. Allais, Levoglucosenone to 3D-printed green materials: synthesizing sustainable and tunable monomers for eco-friendly photo-curing, *Green Chem.*, 2023, **25**, 7571–7581.
10 T. Debsharma, Y. Yagci and H. Schlaad, Cellulose–Derived Functional Polyacetal by Cationic Ring–Opening Polymerization of Levoglucosenyl Methyl Ether, *Angew. Chem., Int. Ed.*, 2019, **58**, 18492–18495.
11 P. Dey and Z. Witczak, Functionalized S-Thio-di- and S-Oligosaccharide Precursors as Templates for Novel SLe x/a Mimetic Antimetastatic Agents, *Mini-Rev. Med. Chem.*, 2003, **3**, 271–280.
12 J. E. Camp and B. W. Greatrex, Levoglucosenone: Bio-Based Platform for Drug Discovery, *Front. Chem.*, 2022, **10**, 902239.
13 T. Debsharma, Y. Yagci and H. Schlaad, Cellulose–Derived Functional Polyacetal by Cationic Ring–Opening Polymerization of Levoglucosenyl Methyl Ether, *Angew. Chem.*, 2019, **131**, 18663–18666.
14 J. E. Camp and B. W. Greatrex, Levoglucosenone: Bio-Based Platform for Drug Discovery, *Front. Chem.*, 2022, **10**, 902239.
15 S. Fadlallah, L. M. M. Mouterde, G. Garnier, K. Saito and F. Allais, in *ACS Symposium Series*, ed. H. N. Cheng and R. A. Gross, American Chemical Society, Washington, DC, 2020, vol. 1373, pp. 77–97.
16 J. Kühlborn, J. Groß and T. Opatz, Making natural products from renewable feedstocks: back to the roots?, *Nat. Prod. Rep.*, 2020, **37**, 380–424.

17 J. A. Galbis, M. D. G. García-Martín, M. V. De Paz and E. Galbis, Synthetic Polymers from Sugar-Based Monomers, *Chem. Rev.*, 2016, **116**, 1600–1636.
18 M. G. Banwell, X. Liu, L. A. Connal and M. G. Gardiner, Synthesis of Functionally and Stereochemically Diverse Polymers via Ring-Opening Metathesis Polymerization of Derivatives of the Biomass-Derived Platform Molecule Levoglucosenone Produced at Industrial Scale, *Macromolecules*, 2020, **53**, 5308–5314.
19 B. Pollard, M. G. Gardiner, M. G. Banwell and L. A. Connal, Polymers from Cellulosic Waste: Direct Polymerization of Levoglucosenone using DBU as a Catalyst, *ChemSusChem*, 2024, **17**, e202301165.
20 J. Baranwal, B. Barse, A. Fais, G. L. Delogu and A. Kumar, Biopolymer: A Sustainable Material for Food and Medical Applications, *Polymers*, 2022, **14**, 983.
21 M. K. Stanfield, R. S. Terry, J. A. Smith and S. C. Thickett, Levoglucosan and levoglucosenone as bio-based platforms for polymer synthesis, *Polym. Chem.*, 2023, **14**, 4949–4956.
22 M. P. Timilsina, M. K. Stanfield, J. A. Smith and S. C. Thickett, Synthesis and Characterization of Thiol–Ene Networks Derived from Levoglucosenone, *ChemPlusChem*, 2024, e202400383.
23 L. Pezzana, S. Fadlallah, G. Giri, C. Archimbaud, I. Roppolo, F. Allais and M. Sangermano, DLP 3D Printing of Levoglucosenone–Based Monomers: Exploiting Thiol–ene Chemistry for Bio–Based Polymeric Resins, *ChemSusChem*, 2024, e202301828.
24 M. K. Porwal, M. M. Hausladen, C. J. Ellison and T. M. Reineke, Biobased and degradable thiol–ene networks from levoglucosan for sustainable 3D printing, *Green Chem.*, 2023, **25**, 1488–1502.
25 E. A. Prebihalo, M. Johnson and T. M. Reineke, Bio-Based Thiol–ene Network Thermosets from Isosorbide and Terpenes, *ACS Macro Lett.*, 2024, **13**, 586–591.
26 H. Şeker and E. Çakmakçi, Fully bio–based thiol–ene photocured thermosets from isosorbide and tung oil, *J. Polym. Sci.*, 2020, **58**, 1105–1114.
27 L. Pezzana, G. Melilli, P. Delliere, D. Moraru, N. Guigo, N. Sbirrazzuoli and M. Sangermano, Thiol-ene biobased networks: Furan allyl derivatives for green coating applications, *Prog. Org. Coat.*, 2022, **173**, 107203.
28 F. C. M. Scheelje and M. A. R. Meier, Non-isocyanate polyurethanes synthesized from terpenes using thiourea organocatalysis and thiol-ene-chemistry, *Commun. Chem.*, 2023, **6**, 239.
29 L. Shahzadi, F. Maya, M. C. Breadmore and S. C. Thickett, Functional Materials for DLP-SLA 3D Printing Using Thiol–Acrylate Chemistry: Resin Design and Postprint Applications, *ACS Appl. Polym. Mater.*, 2022, **4**, 3896–3907.
30 M. Uygun, M. A. Tasdelen and Y. Yagci, Influence of Type of Initiation on Thiol–Ene "Click" Chemistry, *Macromol. Chem. Phys.*, 2010, **211**, 103–110.
31 N. B. Cramer, T. Davies, A. K. O'Brien and C. N. Bowman, Mechanism and Modeling of a Thiol–Ene Photopolymerization, *Macromolecules*, 2003, **36**, 4631–4636.
32 M. J. Kade, D. J. Burke and C. J. Hawker, The power of thiol–ene chemistry, *J. Polym. Sci., Part A: Polym. Chem.*, 2010, **48**, 743–750.
33 O. Ozukanar, E. Çakmakçi, O. Daglar, H. Durmaz and V. Kumbaraci, Thiol-ene photopolymerization meets azide-alkyne click reactions: P/N/Si-containing, dual curable eugenol-based hybrid coatings, *Eur. Polym. J.*, 2023, **195**, 112203.
34 A. L. Flourat, L. Pezzana, S. Belgacem, A. Dosso, M. Sangermano, S. Fadlallah and F. Allais, Levoglucosenone to 3D-printed green materials: synthesizing sustainable and tunable monomers for eco-friendly photo-curing, *Green Chem.*, 2023, **25**, 7571–7581.
35 E. Hernández, M. A. Mosiewicki and N. E. Marcovich, Bio–Based Polymers Obtained from Modified Fatty Acids and Soybean Oil with Tailorable Physical and Mechanical Performance, *Eur. J. Lipid Sci. Technol.*, 2020, **122**, 2000182.
36 D. Döpping, J. Kern, N. Rotter, A. Llevot and H. Mutlu, Biogenic Polymeric Materials from Lignocellulosic Biomass-Derivable 4-Pentenoic Acid and Isosorbide for Potential Biomedical Applications, *ACS Sustainable Chem. Eng.*, 2024, **12**, 13401–13408.
37 T. Goculdas, M. Ramirez, M. Crossley, S. Sadula and D. G. Vlachos, Biomass–Derived, Target Specific, and Ecologically Safer Insecticide Active Ingredients, *ChemSusChem*, 2024, **17**, e202400824.
38 X. Ma, N. Anderson, L. V. White, S. Bae, W. Raverty, A. C. Willis and M. G. Banwell, The Conversion of Levoglucosenone into Isolevoglucosenone, *Aust. J. Chem.*, 2015, **68**, 593.
39 M. Lis-Balchin and G. Roth, Citronellic Acid: A Major Component in Two Pelargonium Species (Geraniaceae), *J. Essent. Oil Res.*, 1999, **11**, 83–85.
40 M. L. Hernández, M. D. Sicardo, A. Belaj and J. M. Martínez-Rivas, The Oleic/Linoleic Acid Ratio in Olive (Olea europaea L.) Fruit Mesocarp Is Mainly Controlled by OeFAD2-2 and OeFAD2-5 Genes Together With the Different Specificity of Extraplastidial Acyltransferase Enzymes, *Front. Plant Sci.*, 2021, **12**, 653997.
41 T. E. Clemente and E. B. Cahoon, Soybean Oil: Genetic Approaches for Modification of Functionality and Total Content, *Plant Physiol.*, 2009, **151**, 1030–1040.
42 S. J. Blanksby and G. B. Ellison, Bond Dissociation Energies of Organic Molecules, *Acc. Chem. Res.*, 2003, **36**, 255–263.
43 I. Tarnavchyk, A. Popadyuk, N. Popadyuk and A. Voronov, Synthesis and Free Radical Copolymerization of a Vinyl Monomer from Soybean Oil, *ACS Sustainable Chem. Eng.*, 2015, **3**, 1618–1622.
44 Z. Demchuk, O. Shevchuk, I. Tarnavchyk, V. Kirianchuk, M. Lorenson, A. Kohut, S. Voronov and A. Voronov, Free-Radical Copolymerization Behavior of Plant-Oil-Based Vinyl Monomers and Their Feasibility in Latex Synthesis, *ACS Omega*, 2016, **1**, 1374–1382.

45 M. K. Stanfield, N. Kotlarewski, J. Smith and S. C. Thickett, Biobased Transparent Thiol–Ene Polymer Networks from Levoglucosan, *ACS Appl. Polym. Mater.*, 2024, **6**, 837–845.
46 P. Jia, M. E. Lamm, Y. Sha, Y. Ma, L. Buzoglu Kurnaz and Y. Zhou, Thiol-ene eugenol polymer networks with chemical Degradation, thermal degradation and biodegradability, *Chem. Eng. J.*, 2023, **454**, 140051.
47 Z. Gao, Y. You, Q. Chen, M. North and H. Xie, Vanillin-derived α,ω-diene monomer for thermosets preparation *via* thiol–ene click polymerization, *Green Chem.*, 2023, **25**, 172–182.
48 M. K. Porwal, M. M. Hausladen, C. J. Ellison and T. M. Reineke, Biobased and degradable thiol–ene networks from levoglucosan for sustainable 3D printing, *Green Chem.*, 2023, **25**, 1488–1502.